Neutron scattering off one-neutron halo nuclei in halo effective field theory

Xu Zhang [1,*] Hai-Long Fu [1,2,†] Feng-Kun Guo [1,2,3,‡] and Hans-Werner Hammer [4,5,§]

[1]*CAS Key Laboratory of Theoretical Physics, Institute of Theoretical Physics, Chinese Academy of Sciences, Beijing 100190, China*
[2]*School of Physical Sciences, University of Chinese Academy of Sciences, Beijing 100049, China*
[3]*Peng Huanwu Collaborative Center for Research and Education, Beihang University, Beijing 100191, China*
[4]*Institut für Kernphysik, Technische Universität Darmstadt, 64289 Darmstadt, Germany*
[5]*ExtreMe Matter Institute EMMI and Helmholtz Forschungsakademie Hessen für FAIR (HFHF), GSI Helmholtzzentrum für Schwerionenforschung GmbH, 64291 Darmstadt, Germany*

(Received 30 August 2023; accepted 22 September 2023; published 9 October 2023)

Neutron scattering off neutron halos can provide important information about the internal structure of nuclei close to the neutron drip line. In this work, we use halo effective field theory to study the s-wave scattering of a neutron and the spin-parity $J^P = \frac{1}{2}^+$ one-neutron halo nuclei ^{11}Be, ^{15}C, and ^{19}C at leading order. In the $J = 1$ channel, the only inputs to the Faddeev equations are their one-neutron separation energies. In the $J = 0$ channel, the neutron-neutron scattering length and the two-neutron separation energies of ^{12}Be, ^{16}C, and ^{20}C enter as well. The numerical results show that the total s-wave cross sections in the $J = 1$ channel at threshold are of the order of a few barns. In the $J = 0$ channel, these cross sections are of the order of a few barns for n-^{11}Be and n-^{19}C scattering, and about 60 mb for the n-^{15}C scattering. The appearance of a pole in $p\cot\delta$ close to zero in all three cases indicates the existence of a virtual Efimov state close to threshold in each of the ^{12}Be, ^{16}C, and ^{20}C systems. Observation of this pole would confirm the presence of Efimov physics in halo nuclei. The dependence of the results on the neutron-core scattering length is also studied.

DOI: 10.1103/PhysRevC.108.044304

I. INTRODUCTION

Over the last four decades, various nuclei have been discovered where the valence neutron(s) have a large probability to distribute in the classically forbidden region outside the range of the core potential [1–4]. To a good approximation, these nuclei can be described as a compact, structureless core surrounded by a halo of valence neutron(s). The unusual size of the halo nuclei can be viewed as a consequence of quantum mechanical tunneling of the halo neutrons out of the core potential. Understanding the structure of halo nuclei provides a window to fundamental aspects of the nuclei along the neutron drip line.

Effective field theory (EFT) provides a powerful tool to explore nuclear systems where the separation of scales exists [5,6]. Depending on the desired resolution scale, different EFTs for nuclear phenomena have been constructed (see Refs. [7–17] for reviews of these efforts). In an EFT, one can construct the most general Lagrangian involving low-energy degrees of freedom while the short-distance physics can be described by a derivative expansion of local interactions. Physical observables can be expanded in powers of the short-distance over large-distance scales. EFT allows a systematic and controlled approach to investigating nuclear interactions in low-energy processes. The separation of scales in halo nuclei implies that one can use an EFT for halo nuclei (the so-called halo EFT), which uses the core and the halo nucleons as degrees of freedom [18–20]. Their interaction is described by contact terms expanded in powers of Q/Λ, where Q is a general low-energy momentum scale, while Λ is the breakdown scale of halo EFT. It is set by the lowest scale of physics not explicitly included, such as the pion mass $m_\pi \approx 140$ MeV or the momentum corresponding to a core excitation. In halo EFT, the core and valence neutron(s) are treated as point-like particles. The finite size of the core enters only in higher-order corrections.

Halo EFT has been used to study a variety of processes. The theory was first applied to study the shallow p-wave neutron-α resonance [18,19] and the s-wave α-α resonance [20]. Then, it was extended to investigate three-body systems. For example, the structure of two-neutron halo nuclei and the relevance of the Efimov effect [21–29] were studied at leading order (LO) in Refs. [30–34] and next-to-leading order (NLO) in Refs. [35,36]. Halo EFT has also been used to study the electromagnetic reactions of neutron and proton halo nuclei including range corrections and higher-order electromagnetic interactions (see, e.g., Refs. [37–44]).

*zhangxu@itp.ac.cn
†fuhailong@itp.ac.cn
‡fkguo@itp.ac.cn
§hans-werner.hammer@physik.tu-darmstadt.de

Reviews of the applications of halo EFT can be found in Refs. [16,45].

The halos ^{11}Be, ^{15}C, and ^{19}C with spin-parity $J^P = \frac{1}{2}^+$ all have a core with $J^P = 0^+$. The lowest excitation energies E_c^* of the cores ^{10}Be, ^{14}C, and ^{18}C are 3.368, 6.094, and 1.62 MeV according to the Triangle Universities Nuclear Laboratory (TUNL) database [46–49], respectively. Moreover, the one-neutron separation energies B_σ of ^{11}Be, ^{15}C, and ^{19}C are 0.502, 1.218, and 0.58 MeV from the atomic mass evaluation AME2020 [50,51], respectively. A rough estimate of the expansion parameters $Q/\Lambda \sim \sqrt{B_{1n}/E_c^*}$ in halo EFT gives about 0.39 for ^{11}Be, 0.45 for ^{15}C and 0.60 for ^{19}C, respectively. These estimates of the expansion parameter Q/Λ are consistent with an analysis of electromagnetic reactions, as discussed in Refs. [37,39,40,52,53].

Neutron scattering off halo nuclei can provide important information about the internal structure of the nuclei in the neutron drip line region. Such experiments may be performed with radioactive beams of the halo nuclei [54–58] on a deuterium target. The reactions can be computed from the neutron-halo and proton-halo scattering amplitudes. In principle, they may also be performed directly at facilities with neutron beams, such as the China Spallation Neutron Source (CSNS) [59,60], if appropriate beams of the halo nuclei become available.

In this work, we study the interaction of the neutron and the spin-parity $J^P = \frac{1}{2}^+$ one-neutron halo nuclei ^{11}Be, ^{15}C, and ^{19}C using halo EFT. There are two channels in the s-wave scattering corresponding to the total spin $J = 1$ and $J = 0$. Our calculation is performed at LO. At this order, the only inputs to the Faddeev equations are the one-neutron separation energies of one-neutron halo nuclei in the total spin $J = 1$ channel, as well as the two-neutron scattering length and the two-neutron separation energies of ^{12}Be, ^{16}C, and ^{20}C in the total spin $J = 0$ channel. Corrections from higher orders can be estimated as the theoretical uncertainty.

The paper is organized as follows. In Sec. II, we introduce the effective Lagrangian for the interactions necessary for calculating the scattering of neutron and ^{11}Be, ^{15}C, and ^{19}C. Section III describes how the relevant two-body interactions emerge from the effective Lagrangian. The three-body interactions are studied in Sec. IV. Numerical results and discussions are presented in Sec. V. Finally, we summarize our work in Sec. VI. Some technical details are given in the Appendices.

II. EFFECTIVE LAGRANGIAN

In halo EFT, the relevant degrees of freedom are the core nucleus (c) and the valence nucleon(s). At LO, the two-body subsystems nn and nc are described by zero-range interactions. The effective Lagrangian can be written as a sum of one-body, two-body, and three-body contributions,

$$\mathcal{L} = \mathcal{L}_1 + \mathcal{L}_2 + \mathcal{L}_3. \tag{1}$$

The one-body Lagrangian is

$$\mathcal{L}_1 = \vec{n}^\dagger \left(i\partial_0 + \frac{\nabla^2}{2m_n} \right) \vec{n} + c^\dagger \left(i\partial_0 + \frac{\nabla^2}{2m_c} \right) c, \tag{2}$$

TABLE I. The mass of the core nuclei. The data are taken from AME2020 [50,51].

Nuclei	^{10}Be	^{14}C	^{18}C
m_c (MeV)	9327.5	13043.9	16791.8

where c is a scalar field for the core nuclei ^{10}Be, ^{14}C, and ^{18}C with a mass m_c, the masses are taken from Refs. [50,51] as given in Table I, and $\vec{n}$ represents a two-component spinor field of the valence neutron $\vec{n} = (n_\uparrow \;\; n_\downarrow)$ with a mass m_n. The mass of neutron is taken to be $m_n = 939.57$ MeV [61]. If the effective ranges are positive, the two-body Lagrangian involving the s-wave nn and nc interactions to NLO can be written as [37,40,62–64]

$$\begin{aligned}\mathcal{L}_2 = {} & s^\dagger \left[\Delta_s - \left(i\partial_0 + \frac{\nabla^2}{4m_n} \right) \right] s \\ & + \sigma_i^\dagger \left[\Delta_\sigma - \left(i\partial_0 + \frac{\nabla^2}{2m_\sigma} \right) \right] \sigma_i \\ & - g_s C^{00}_{1/2\alpha,1/2\beta} [s^\dagger n_\alpha n_\beta + \text{H.c.}] - g_\sigma [\sigma_i^\dagger n_i c + \text{H.c.}],\end{aligned} \tag{3}$$

where s is a scalar dimer field for the two-neutron system, $\vec{\sigma} = (\sigma_\uparrow \;\; \sigma_\downarrow)$ is a two-component spinor field for ^{11}Be, ^{15}C, and ^{19}C with a mass $m_\sigma = m_c + m_n$, and $C^{00}_{1/2\alpha,1/2\beta}$ is a Clebsch-Gordan coefficient. The parameters Δ_s, Δ_σ, g_s, and g_σ can be determined by experimental data. At LO, $\Delta_{s,\sigma}$ and $g_{s,\sigma}$ are not independent and only the combinations $g^2_{s,\sigma}/\Delta_{s,\sigma}$ enter into observables.

The three-body interaction Lagrangian $\mathcal{L}_3$ can be constructed in terms of the s-wave two-neutron dimer and the core [31,36], which is needed for the renormalization in the total spin $J = 0$ channel at LO. It can be written as

$$\mathcal{L}_3 = g_s^2 D_0 (sc)^\dagger (sc) \tag{4}$$

with D_0 a three-body parameter.

III. TWO-BODY INTERACTIONS

At LO, the bare dimer propagators $i/\Delta_{s,\sigma}$ are dressed by an infinite number of bubble diagrams as shown in Fig. 1. Using the Feynman rules, the full nn and nc dimer propagators consisting of the geometric series represented in Fig. 1 can be

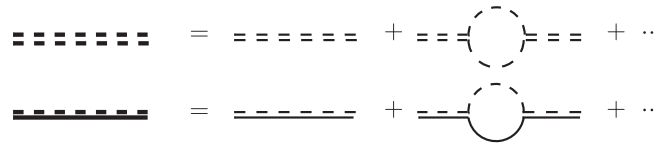

FIG. 1. Dimer propagators at LO from the Lagrangian in Eqs. (3). The double-dashed line and dashed-solid line are the nn and nc propagators, respectively. The bare dimer propagator $i/\Delta_{s,\sigma}$ is dressed by an infinite number of bubble diagrams. The dashed and solid lines represent the neutron and the core nucleus, respectively.

written as

$$iD_s(p_0, p) = \frac{-i}{-\Delta_s + m_n g_s^2/(2\pi)[-\Lambda + \sqrt{m_n[p^2/(4m_n) - p_0 - i\epsilon]}]},$$
$$iD_\sigma(p_0, p) = \frac{-i}{-\Delta_\sigma + \mu_{nc} g_\sigma^2/(2\pi)[-\Lambda + \sqrt{2\mu_{nc}[p^2/(2m_\sigma) - p_0 - i\epsilon]}]}, \quad (5)$$

where p_0 and p are the energy and the magnitude of the three-momentum of the dimer field, respectively. $\mu_{nc} = m_n m_c/(m_n + m_c)$ is the reduced mass of the nc two-body system, and Λ is an arbitrary momentum scale in the power divergence subtraction (PDS) scheme [65,66].

For the nn two-body system, the parameters Δ_s and g_s can be matched to the experimentally known scattering length a_s,

$$a_s^{-1} = \frac{2\pi}{m_n g_s^2}\Delta_s + \Lambda, \quad (6)$$

and we take the value $a_s = -18.6$ fm [67]. The full renormalized nn dimer propagator can then be written as

$$iD_s(p_0, p) = \frac{2\pi}{m_n g_s^2}\frac{-i}{-1/a_s + \sqrt{m_n[p^2/(4m_n) - p_0 - i\epsilon]}}. \quad (7)$$

For a negative scattering length a_s, the pole of the propagator is on the second Riemann sheet of the complex energy plane and the residue at the pole is negative,

$$Z_s^{-1} = \frac{m_n^2 g_s^2 a_s}{4\pi}. \quad (8)$$

For the nc two-body system, the parameters Δ_σ and g_σ are connected to the scattering length a_σ by

$$a_\sigma^{-1} = \frac{2\pi}{\mu_{nc} g_\sigma^2}\Delta_\sigma + \Lambda, \quad (9)$$

and the full renormalized nc dimer propagator can then be written as

$$iD_\sigma(p_0, p) = \frac{2\pi}{\mu_{nc} g_\sigma^2}\frac{-i}{-1/a_\sigma + \sqrt{2\mu_{nc}[p^2/(2m_\sigma) - p_0 - i\epsilon]}}. \quad (10)$$

The nc dimer propagator has a pole at

$$p_0 - \frac{p^2}{2m_\sigma} = -\frac{1}{2\mu_{nc} a_\sigma^2} = -B_\sigma, \quad (11)$$

where B_σ is the separation energy between the core and the valence neutron of the one-neutron halo nucleus. The input parameters for the nc two-body interaction are given in Table II. For positive scattering length a_σ, the pole of the propagator is on the first Riemann sheet of the complex square root and the residue at the pole is positive,

$$Z_\sigma^{-1} = \frac{\mu_{nc}^2 g_\sigma^2 a_\sigma}{2\pi}. \quad (12)$$

In our calculation, we stay at LO in the power counting of halo EFT, and the effective range corrections arising from the kinetic terms of the dimers in Eq. (3) are not included [68–71].

TABLE II. EFT inputs for the nc two-body interactions. The data are taken from AME2020 [50,51].

Halo nuclei	^{11}Be	^{15}C	^{19}C
B_σ (MeV)	0.502	1.218	0.58
a_σ (fm)	6.741	4.27	6.142

IV. THREE-BODY INTERACTION

In this work, we are interested in the s-wave scattering of the neutron and the one-neutron halo nuclei ^{11}Be, ^{15}C, and ^{19}C in halo EFT. The Efimov effect appears in three-body systems when the scattering length of the two-body subsystem is much larger than the range of the forces [21–26,28]. The condition for the appearance of the Efimov state in halo nuclei was first studied in Ref. [25]. The Efimov effect in ^{12}Be and ^{20}C was studied in the renormalized zero-range model in Ref. [27]. In Refs. [30,35] it was investigated in halo EFT at LO and NLO. Taking the values of the nc two-body binding energy B_σ from the TUNL database [47–49], the numerical calculations at LO indicate that only ^{20}C with the n-^{18}C bound state energy $B_\sigma = (0.162 \pm 0.112)$ MeV has a possible excited Efimov state, with an energy less than 14 keV in Ref. [27] and 7 keV in Ref. [30] below the n-^{19}C threshold. The shift in the excited state binding energy is found less than 0.5 keV at NLO in Ref. [35]. However, recent evaluation in AME2020 [50,51] finds $B_\sigma = (0.58 \pm 0.09)$ MeV for the n-^{18}C interaction, which does not support an excited Efimov state in ^{20}C. Experiments on neutron scattering off halo nuclei provide important information about the internal structure of the nuclei, and can put constraints on the possible existence of excited Efimov states in these nuclei.

The radius of halo nuclei is much larger than the radius of their core, and the core can be assumed as point-like. This separation of scales allows for a description of the low-energy properties of halo nuclei using contact interactions between the halo neutrons and between the neutrons and the core. The T matrix for scattering of a neutron and a one-neutron halo nucleus will be calculated at LO in halo EFT, by solving the corresponding Faddeev integral equation. The integral equation was first derived in Ref. [72] for the neutron-deuteron system and is identical to the result given in Ref. [73] if contact interactions are considered. Including only two-body interactions, the numerical results for s-wave observables in the three-body system of two neutrons and the core nucleus in the total spin $J = 0$ channel, where three-body bound states appear, suffer from a peculiar cutoff dependence. This behavior was already observed in Refs. [74–76] for the $J = 1/2$

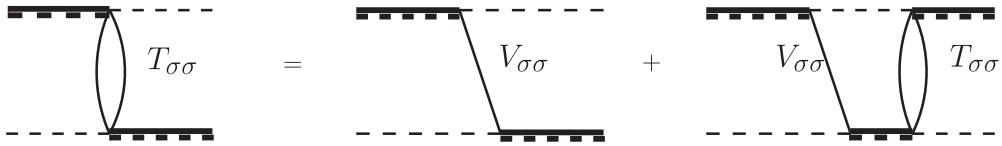

FIG. 2. Faddeev equation for the $n\sigma$ scattering in the total spin $J = 1$ channel at LO. The notations are the same as those in Fig. 1.

neutron deuteron system and also occurs in the three-boson system. This cutoff dependence can be removed by introducing a three-body force that runs log-periodically with the cutoff [64,77,78]. Fixing the three-body force from a single three-body observable, all other observables can be predicted at LO. In our calculations, the three-body forces in the $J = 0$ channel are fixed with the ^{12}Be, ^{16}C, and ^{20}C ground state two-neutron separation energies, and the log-periodic behavior of the three-body forces is also observed as expected (see below).

A. Total spin $J = 1$ channel

The T matrix for lth partial wave $n\sigma$ scattering in the total spin $J = 1$ channel is given by the integral equation displayed in Fig. 2. Since the spin of the core nucleus of interest is zero, the total spin of the two neutrons should be one for this channel. Such a configuration is not forbidden by the Pauli exclusion principle because one of the neutrons is bound inside the neutron halo nucleus. Thus the identical fermions are not localized in a point. Three-body contact terms without derivatives, however, are forbidden by the exclusion principle. Indeed one finds that no three-body force contribution at LO is needed to achieve a cutoff independent solution. The integral equation for this channel can be written as

$$iT^{l}_{\sigma\sigma}(k,p,E) = iV^{l}_{\sigma\sigma}(k,p,E) - \int_0^\Lambda \frac{q^2 dq}{2\pi^2} V^{l}_{\sigma\sigma}(k,q,E) \times Z_\sigma^{-1} D_\sigma\left(E - \frac{q^2}{2m_n}, q\right) iT^{l}_{\sigma\sigma}(q,p,E), \tag{13}$$

where p and k are the magnitudes of the incoming and outgoing momenta of the spectator neutron in the three-body center-of-mass frame, respectively, and the upper index l denotes the partial wave. The total nonrelativistic on-shell energy is

$$E = \frac{p^2}{2\mu_{n\sigma}} - \frac{1}{2\mu_{nc}a_\sigma^2} = \frac{p^2}{2\mu_{n\sigma}} - B_\sigma, \tag{14}$$

where

$$\mu_{n\sigma} = \frac{m_n m_\sigma}{m_n + m_\sigma} \tag{15}$$

is the $n\sigma$ reduced mass. Notice that when all external legs are on-shell, the momenta p and k are equal.

The lth partial wave projection of the core-exchange potential can be written as

$$\begin{aligned} V^{l}_{\sigma\sigma}(k,q,E) &= Z_\sigma g_\sigma^2 \cdot \frac{1}{2}\int_{-1}^{+1} \frac{P_l(\cos\theta)\, d\cos\theta}{E - k^2/(2m_n) - q^2/(2m_n) - (\vec{q}+\vec{k})^2/(2m_c) + i\epsilon}, \\ &= Z_\sigma g_\sigma^2 \cdot \frac{m_c}{qk} Q_l\left(\frac{m_c E - m_\sigma/(2m_n)(q^2+k^2) + i\epsilon}{qk}\right), \end{aligned} \tag{16}$$

where θ is the angle between $\vec{q}$ and $\vec{k}$, the Legendre polynomial of the second kind with complex argument is

$$Q_l(z) = \frac{1}{2}\int_{-1}^{+1} \frac{P_l(\cos\theta)\, d\cos\theta}{z - \cos\theta}, \tag{17}$$

and the analytic expressions of the first few $Q_l(z)$ are given in Appendix A.

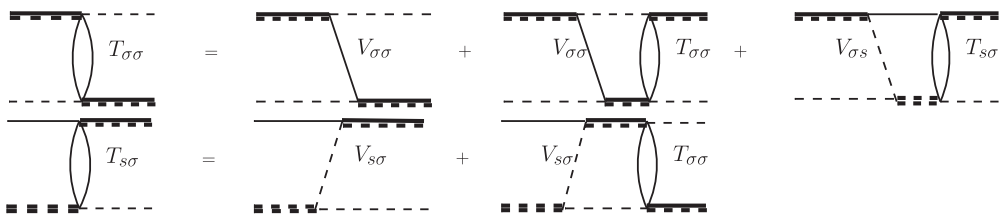

FIG. 3. Faddeev equation for the $n\sigma$ scattering in the total spin $J = 0$ channel at LO. The notations are the same as those in Fig. 1.

B. Total spin $J = 0$ channel

The T matrix for the lth partial wave $n\sigma$ scattering in the total spin $J = 0$ channel is given by the integral equation shown in Fig. 3. The integral equation for this channel can be written as

$$\begin{pmatrix} iT^l_{\sigma\sigma}(k,p,E) \\ iT^l_{s\sigma}(k,p,E) \end{pmatrix} = \begin{pmatrix} -iV^l_{\sigma\sigma}(k,p,E) \\ i2V^l_{s\sigma}(k,p,E) \end{pmatrix} - \int_0^\Lambda \frac{q^2 dq}{2\pi^2} \begin{pmatrix} -V^l_{\sigma\sigma}(k,q,E) & 2V^l_{\sigma s}(k,q,E) \\ 2V^l_{s\sigma}(k,q,E) & 0 \end{pmatrix} \times \begin{pmatrix} Z_\sigma^{-1} D_\sigma\left(E - \frac{q^2}{2m_n}, q\right) & 0 \\ 0 & Z_s^{-1} D_s\left(E - \frac{q^2}{2m_c}, q\right) \end{pmatrix} \begin{pmatrix} iT^l_{\sigma\sigma}(q,p,E) \\ iT^l_{s\sigma}(q,p,E) \end{pmatrix}. \tag{18}$$

The lth partial wave projection of the core-exchange potential has been given in Eq. (16). The lth partial wave projection of the neutron-exchange potential can be written as

$$\begin{aligned} V^l_{\sigma s}(k,q,E) &= (\sqrt{Z_\sigma Z_s} g_\sigma g_s) \cdot \frac{1}{2} \int_{-1}^{+1} \frac{P_l(\cos\theta) d\cos\theta}{E - k^2/2m_n - q^2/2m_c - (\vec{q}+\vec{k})^2/2m_n + i\epsilon}, \\ &= (\sqrt{Z_\sigma Z_s} g_\sigma g_s) \cdot \frac{m_n}{qk} Q_l\left(\frac{m_n E - k^2 - m_\sigma/(2m_c) q^2 + i\epsilon}{qk}\right), \end{aligned} \tag{19}$$

and

$$V^l_{s\sigma}(k,q,E) = V^l_{\sigma s}(q,k,E). \tag{20}$$

For this channel, a three-body force is required for renormalization at LO. For clarity, however, the three-body force terms are omitted in Fig. 3 and Eq. (18). Their contribution will be included in the calculations below.

The integral equations in the $J = 0$ and $J = 1$ channels are solved numerically. Details of the numerical solution method are given in Appendix B.

V. NUMERICAL RESULTS AND DISCUSSION

At LO of halo EFT, the only input parameter in the $J = 1$ channel is the neutron-core s-wave scattering length or the one-neutron separation energy of the one-neutron-halo nucleus. The values for the ^{11}Be, ^{15}C, and ^{19}C nuclei are listed in Table II. In addition, to understand the dependence of the results from the variation of the nc scattering length a_σ, its values will be varied by ± 0.5 fm. In the $J = 0$ channel, two additional parameters are needed to fix the interactions: the two-neutron scattering length a_s and the two-neutron separation energies B_{2n} of ^{12}Be, ^{16}C, and ^{20}C to fix the three-body force. We use the values given in the AME2020 [50,51] as shown in Table III.

A. Cutoff dependence in the $J = 0$ channel

Using a sharp cutoff Λ to regularize the Faddeev equation in Eq. (18) and omitting the three-body force, the cutoff dependence of the three-body binding energies in the $J = 0$ channel are shown in Fig. 4. One can see that the energies have a strong cutoff dependence. Asymptotically, they grow with Λ^2. In addition, the binding energies are insensitive to the masses of different nuclei for the given scattering lengths a_σ. This fact can be expected as the core nuclei considered here are much heavier than the neutron, and thus the core kinetic energies are much smaller than that of the neutron.[1]

Following Refs. [30,77], one may add a three-body counterterm to the Faddeev equation (18) to cancel this cutoff dependence,

$$V_{ss}(k,p,E) = Z_s g_s^2 D_0. \tag{21}$$

TABLE III. Two-neutron separation energies B_{2n}. The data are taken from AME2020 [50,51].

Halo nuclei	^{12}Be	^{16}C	^{20}C
B_{2n} (MeV)	3.672	5.468	3.560

[1]When the core nucleus is much heavier than the nucleon, one may construct an EFT treating the core nucleus as static at LO, similar to the heavy quark effective theory [79] and heavy baryon chiral perturbation theory [80,81].

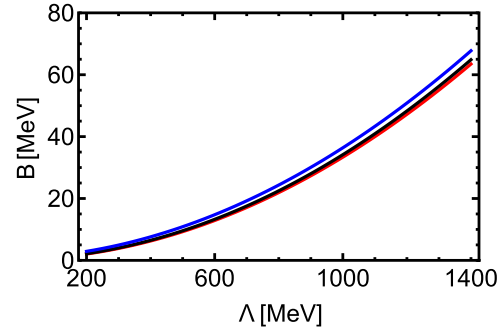

FIG. 4. Cutoff dependence of the three-body binding energy in the $J = 0$ channel without a three-body counterterm. The red, blue, and black lines correspond to the bound states generated from the nn ^{10}Be, nn ^{14}C, and nn ^{18}C three-body interactions, respectively.

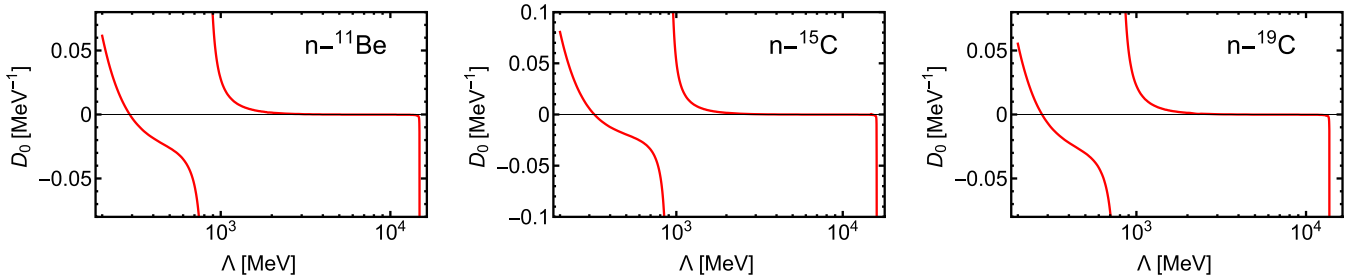

FIG. 5. The three-body parameter D_0 as a function of the cutoff Λ. D_0 is tuned to reproduce the ground state two-neutron separation energy for each of ^{12}Be (left), ^{16}C (middle), and ^{20}C (right).

The counterterm parameter D_0 is tuned to reproduce the ground state two-neutron separation energy for each of ^{12}Be, ^{16}C, and ^{20}C. Once this renormalization is done, all other three-body observables, such as scattering cross sections are also cutof independent. The cutoff dependence of the three-body parameter D_0 is shown in Fig. 5. One can see that the three-body parameter D_0 has a quasiperiodic behavior in ln Λ. Similar to the three-boson case [77,82], the function $\Lambda^2 D_0$ is log-periodic in Λ (see Ref. [16] for a detailed investigation of this behavior for different core masses).

B. Amplitudes and total cross sections in the $J = 1$ channel

The on-shell amplitudes for scattering of neutrons from the neutron halo nuclei, T, are related to the scattering phase shifts through the relation

$$T^{l}_{\sigma\sigma}(p, p, E) = \frac{2\pi}{\mu_{n\sigma}} \frac{1}{p \cot \delta_l(p) - ip}, \tag{22}$$

where the reduced mass $\mu_{n\sigma}$ is defined in Eq. (15). The differential cross section for a given spin state in terms of the phase shifts can be written as [83]

$$\frac{d\sigma}{d\Omega} = \sum_l \left| \frac{2l+1}{p \cot \delta_l(p) - ip} P_l(\cos\theta) \right|^2. \tag{23}$$

Then the total cross section is

$$\sigma(p, p, E) = \sum_l \frac{(2l+1)\mu^2_{n\sigma}}{\pi} |T^{l}_{\sigma\sigma}(p, p, E)|^2. \tag{24}$$

In the $J = 1$ channel, no three-body bound states in the nn^{10}Be, nn^{14}C, and nn^{18}C systems exist. The equations for the amplitudes of n-^{11}Be, n-^{15}C, and n-^{19}C scattering have a unique solution as $\Lambda \to \infty$. We take the values in Table II as input for the the nc scattering length a_σ and vary it by ± 0.5 fm to show the dependence of the results on this input. The results of $p \cot \delta_0(p)$ for the s-wave scattering defined in Eq. (22) are shown in Fig. 6. One can see that $p \cot \delta_0(p)$ [and also the phase shift $\delta_0(p)$] is real below the breakup threshold of the one-neutron halo nucleus and develops a small imaginary part above since the neutron-core continuum channel is open. The real part of $p \cot \delta_0(p)$ is essentially constant over the full range of p considered, resulting in a very small $n\sigma$ effective range. Finally, the results depend only weakly on a_σ.

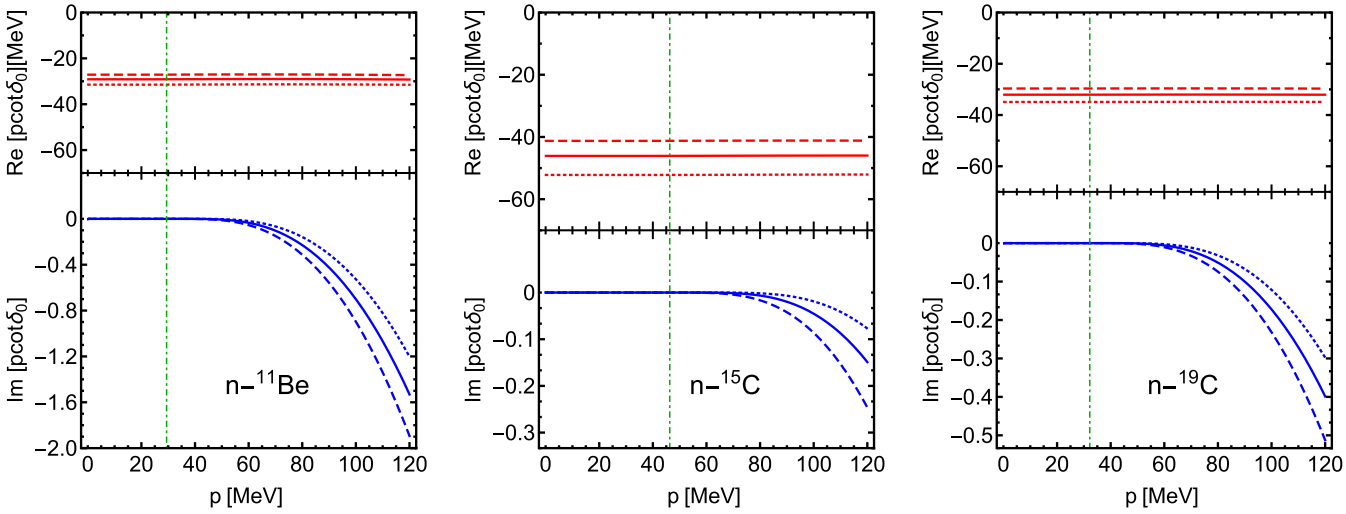

FIG. 6. Real and imaginary parts of $p \cot \delta_0(p)$ for the s-wave scattering of neutron and one-neutron halo nuclei in the $J = 1$ channel. The left, middle, and right panels correspond to the n-^{11}Be, n-^{15}C, and n-^{19}C scattering processes, respectively. The solid lines represent the results using the scattering lengths a_σ in Table II as inputs, while the dashed/dotted curves correspond to $a_\sigma \pm 0.5$ fm, respectively. The vertical dot-dashed lines in the plots indicate the threshold for breakup into the neutron core continuum.

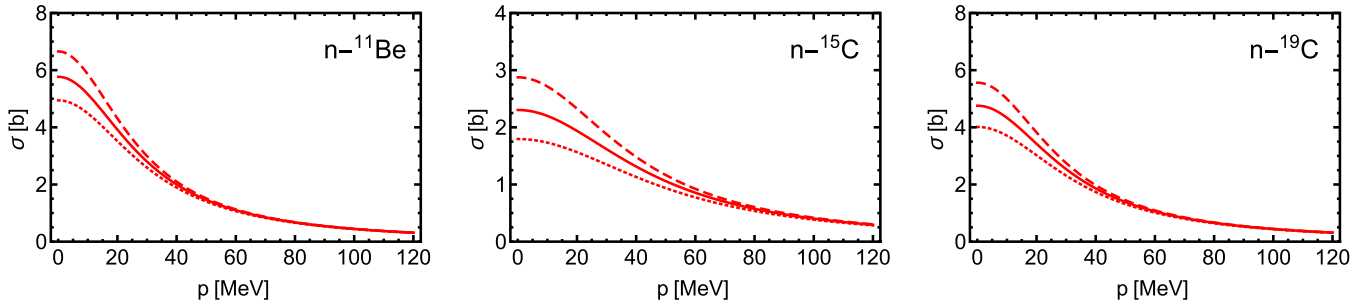

FIG. 7. The total s-wave cross sections for the scattering of neutron and one-neutron halo nuclei in the $J = 1$ channel: n-^{11}Be (left), n-^{15}C (middle), and n-^{19}C (right). The notations of the solid, dashed, and dotted curves are the same as those in Fig. 6.

The total s-wave scattering cross sections σ are shown in Fig. 7. One can see that there is a bump at threshold in each of the total cross sections of the n-^{11}Be, n-^{15}C, and n-^{19}C scattering processes, and the total cross sections have a small change in the ranges of a_σ we considered. Our numerical results suggest that the total cross sections at threshold are of the order of a few barns for the n-^{11}Be, n-^{15}C, and n-^{19}C scattering.

C. Amplitudes and total cross sections in the $J = 0$ channel

In the $J = 0$ channel, the amplitudes of the n-^{11}Be, n-^{15}C, and n-^{19}C scattering do not have a unique solution as $\Lambda \to \infty$ if the D_0 term in Eq. (4) is neglected. For finite Λ, they display a strong cutoff dependence. The three-body counterterm D_0 is required for renormalization, as discussed in Sec. V A, and the value for each of the ^{12}Be, ^{16}C, and ^{20}C systems is fixed through the two-neutron separation energies listed in Table III.

The results for the s-wave scattering $p\cot\delta_0(p)$ in the $J = 0$ case are shown in Fig. 8, where the solid lines represent the results using the a_σ values in Table II as inputs and the dashed (dotted) lines correspond to those obtained by increasing (decreasing) a_σ by 0.5 fm.

The values of $p\cot\delta_0(p)$ are real below the threshold for breakup of the one-neutron halo nuclei in the scattering process. They become complex above since the breakup channel is open, and compared to the $J = 1$ channel the imaginary parts of $p\cot\delta_0(p)$ are much larger. Alternatively, the on-shell amplitudes T can be related to real-valued scattering phase shifts $\delta_l^R(p)$ through the relation

$$T^l_{\sigma\sigma}(p, p, E) = \frac{2\pi}{\mu_{n\sigma}} \frac{\eta e^{2i\delta_l^R(p)} - 1}{2ip} \tag{25}$$

with η as the inelasticity factor. With this definition $\eta = 1$ below the breakup threshold and $0 \leqslant \eta < 1$ above. Thus a large inelasticity corresponds to small values of η. Our results for η are shown in Fig. 9. The inelasticity grows rapidly when the momentum p is increased beyond the breakup threshold.

The most interesting feature of our results is that for all the considered processes, there is a pole in $p\cot\delta_0^R(p)$, and thus a zero of the T matrix when this pole is below the breakup threshold. The T matrix almost vanishes at the pole position when the inelasticity is small. The pole position is sensitive to a_σ. It can be seen from, e.g., the results for n-^{15}C scattering (the middle plot in Fig. 8), that the pole disappears when a_σ

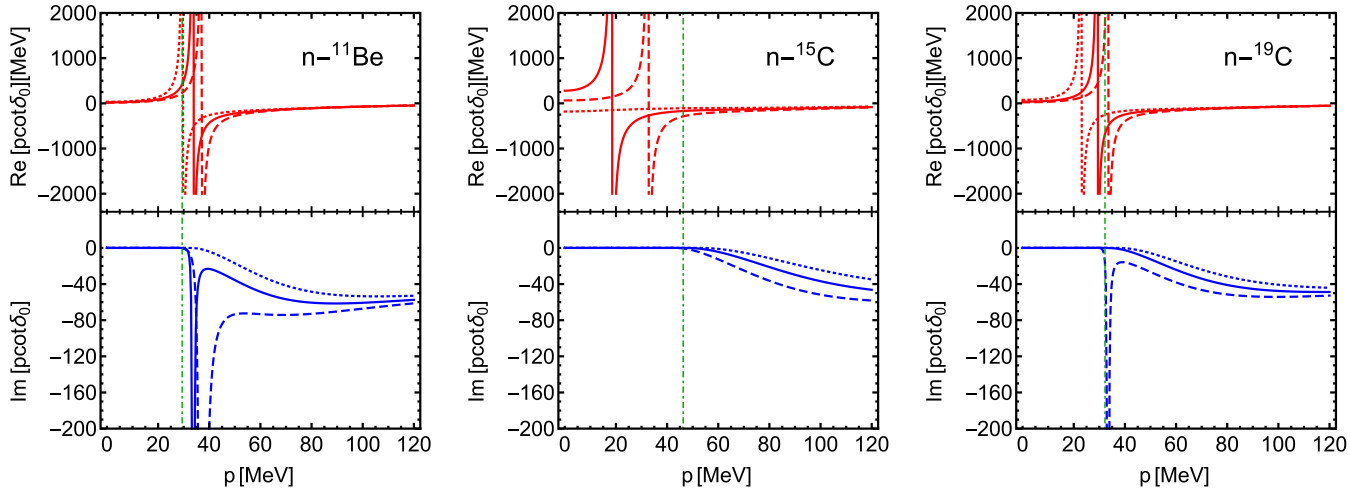

FIG. 8. Real and imaginary parts of $p\cot\delta_0(p)$ for the s-wave scattering of neutron and one-neutron halo nuclei in the $J = 0$ channel. The left, middle, and right panels correspond to the n-^{11}Be, n-^{15}C, and n-^{19}C scattering processes, respectively. The three-body forces are fixed through the two-neutron separation energies of ^{12}Be, ^{16}C, and ^{20}C in Table III. The notations of the solid, dashed, dotted, and dot-dashed lines are the same as those in Fig. 6.

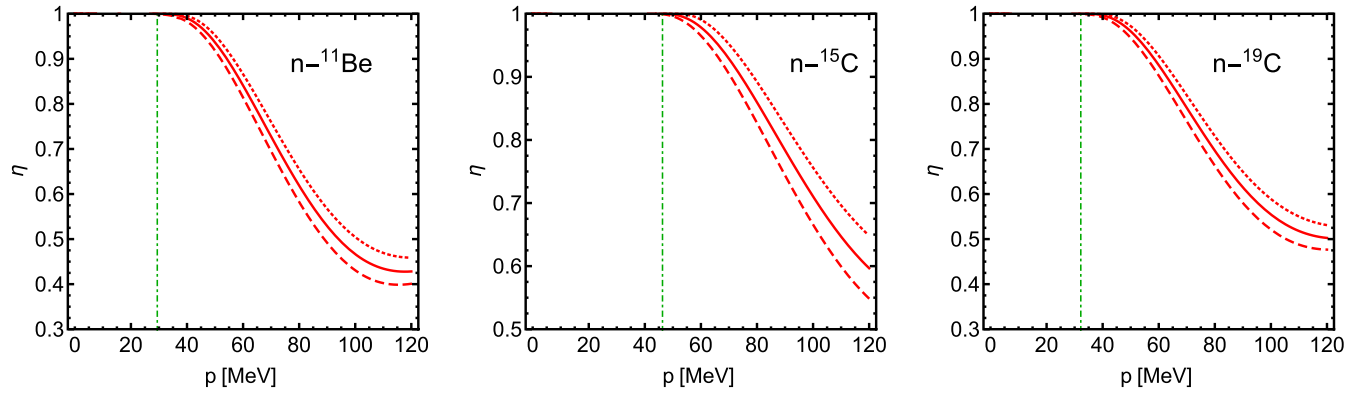

FIG. 9. Inelasticity factor for s-wave scatterings of the neutron and one-neutron halo nuclei in the $J = 0$ channel: n-^{11}Be (left), n-^{15}C (middle), and n-^{19}C (right). The notations of the solid, dashed, dotted, and dot-dashed lines are the same as those in Fig. 6.

decreases from 4.27 fm in Table II to 3.77 fm. Increasing a_σ pushes the pole to larger values of p, as can be seen from Fig. 10 which shows the location of the pole in $p\cot\delta_0^R(p)$ as a function of $1/a_\sigma$. Our results are in qualitative agreement with the findings of Refs. [84–86] for the case of n-^{19}C scattering.

The appearance of this pole indicates the presence of an excited virtual Efimov state close to the scattering threshold. As a_σ is increased the virtual excited state turns into a real excited state that becomes part of the bound state spectrum (this can be understood from, e.g., Fig. 23 of Ref. [28]). Indeed, an excited bound state is found as a_σ is increased. We calculate the value of the excited state energy as a function of $1/a_\sigma$, with the three-body force fixed through the two-neutron separation energies of ^{12}Be, ^{16}C, and ^{20}C in Table III. The dependence of the binding energy of the excited state as a function of $1/a_\sigma$ is plotted in Fig. 11. We find that for ^{12}Be the first excited state appears when a_σ is increased beyond the physical value, viz. $1/a_\sigma \lesssim 16.9$ MeV, while for ^{16}C and ^{20}C the excited state appears for $1/a_\sigma \lesssim 21.5$ MeV and $1/a_\sigma \lesssim 17.2$ MeV, respectively. The appearance of the excited three-body bound state is also signaled by a sign change of the s-wave scattering length for scattering of neutrons from the neutron halo, a, defined as $p\cot\delta_0(p) \overset{p\to 0}{=} -1/a$: a is negative if there is only the three-body ground state of the halo nucleus and turns positive when the virtual three-body state becomes a bound excited state. The results for the s-wave n-^{11}Be, n-^{15}C, and n-^{19}C scattering length a are shown in Fig. 12. Thus the experimental observation of such a pole in $p\cot\delta_0^R(p)$ could serve as a confirmation of Efimov physics in halo nuclei, even if no bound excited state is present. Up to higher order corrections, the energy of the virtual state is completely determined by the ground state energies of the one- and two-neutron halo nuclei under consideration and the neutron-neutron scattering length.

Because of the existence of near-threshold bound states in the $J = 0$ channel for the n-^{11}Be, n-^{15}C, and n-^{19}C systems in question, namely, ^{12}Be, ^{16}C, and ^{20}C, respectively, and virtual excited states, the total cross sections shown as red curves in Fig. 13 have much more prominent threshold enhancement in comparison with those in the $J = 1$ channel shown in Fig. 7. The obtained total cross sections in the near-threshold region are of the order of a few barns for the n-^{11}Be and n-^{19}C scattering and less than 1 barn for the n-^{15}C scattering. The threshold enhancement for the n-^{15}C scattering is milder than

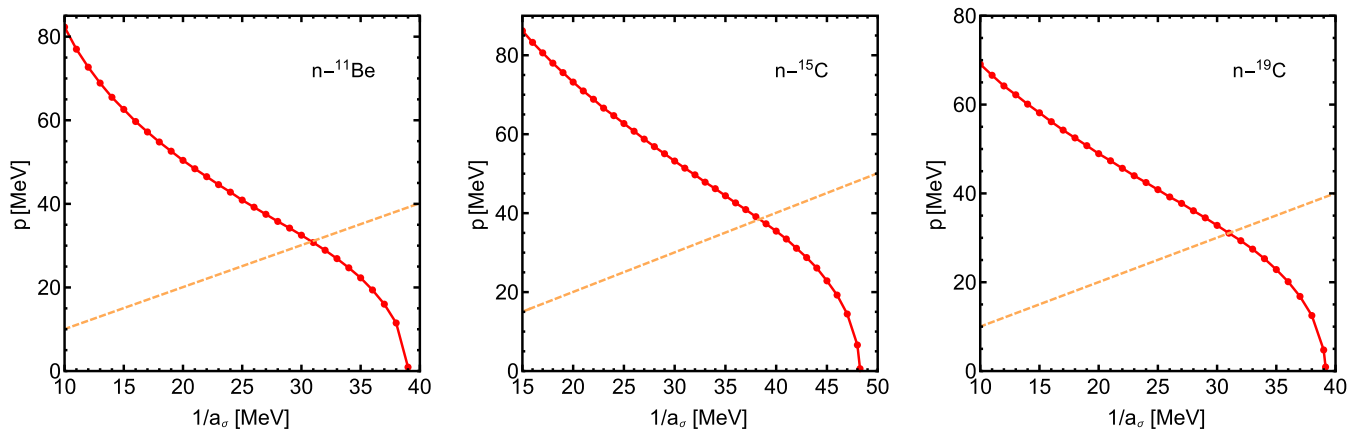

FIG. 10. Location of the pole in $p\cot\delta_0^R(p)$ as a function of $1/a_\sigma$: n-^{11}Be (left), n-^{15}C (middle), and n-^{19}C (right). The dashed line represents the threshold for breakup into the neutron core continuum.

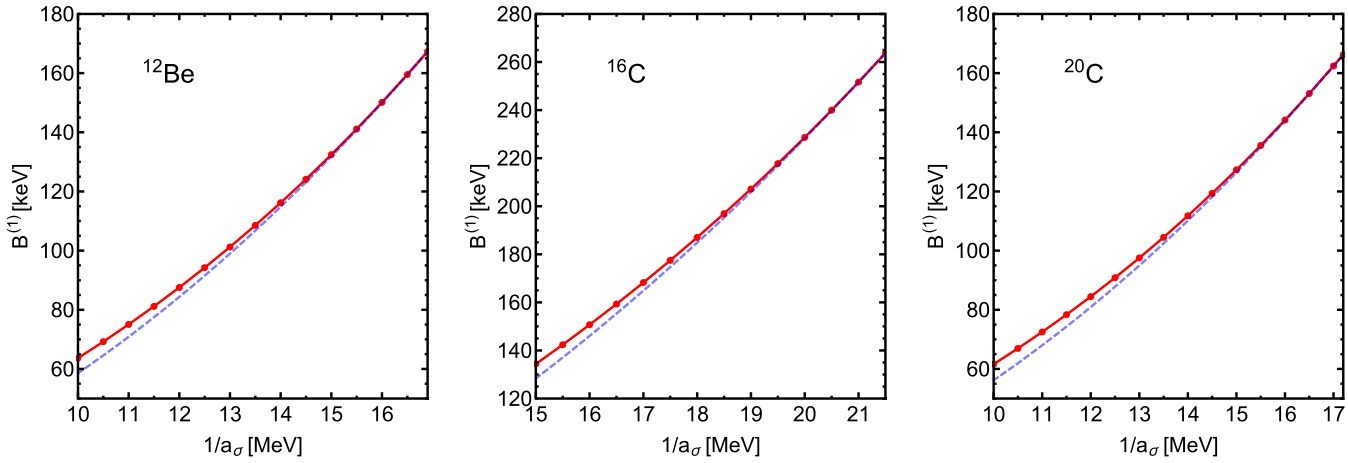

FIG. 11. Binding energy of the excited state as a function of $1/a_\sigma$: ^{12}Be (left), ^{16}C (middle), and ^{20}C (right). The dashed line represents the scattering threshold which is given by $B^{(1)} = B_\sigma$.

the other two cases because the ^{16}C is more deeply bound than the ^{12}Be and ^{20}C (see the two-neutron separation energies in Table III). One also sees that the pole of $p\cot\delta_0^R(p)$ shows up as a zero in the s-wave cross section for each of the considered processes; see the red curves in Fig. 13. We note that this zero in the cross section is an artefact of including only the contribution of s-wave scattering. If the contributions from higher partial waves are included these zeros will be filled up. However, as can be seen from the black curves in Fig. 13, which include contributions with $l < 5$, they remain visible as pronounced minima in the total cross section. The observation of such minima at the predicted positions would provide clear evidence of the Efimov effect in halo nuclei.

Analog phenomena exist in other systems. In a recent study of the double-charm tetraquark T_{cc} in the DD^* scattering with the $DD\pi$ three-body dynamics, a similar pole of $p\cot\delta_0^R(p)$ was also found [87]. In fact, the existence of a similar pole in $p\cot\delta_0^R(p)$ for the neutron-deuteron scattering in the triton channel was already observed more than half a century ago [88,89]. An effective field theory treatment of the excited Efimov state in the triton was presented in Ref. [90].

VI. SUMMARY

In recent years, various halo nuclei with a tightly bound core surrounded by weakly bound valence nucleon(s) have been found. Exploring the structure and reactions of halo nuclei will help us understand fundamental aspects of nuclear forces and nuclei at the edge of stability.

In the present work, the s-wave interactions of neutron and spin-parity $J^P = \frac{1}{2}^+$ one-neutron halo nuclei ^{11}Be, ^{15}C, and ^{19}C are studied using halo EFT at LO. In the total spin $J = 1$ channel, the only input to the Faddeev equation is the one-neutron separation energy for each one-neutron halo nucleus. The total cross sections at threshold are of the order of a few barns for all the considered n-^{11}Be, n-^{15}C, and n-^{19}C scattering processes. In the total spin $J = 0$ channel, the amplitudes of the n-^{11}Be, n-^{15}C, and n-^{19}C scatterings do not have a unique solution as the cutoff $\Lambda \to \infty$. Following Ref. [77] a three-body counterterm D_0 is introduced to absorb the cutoff dependence and to achieve a unique solution of the Faddeev equation. The D_0 values are tuned to reproduce the ^{12}Be, ^{16}C, and ^{20}C ground state two-neutron separation energies. The numerical results show that the total s-wave cross sections at

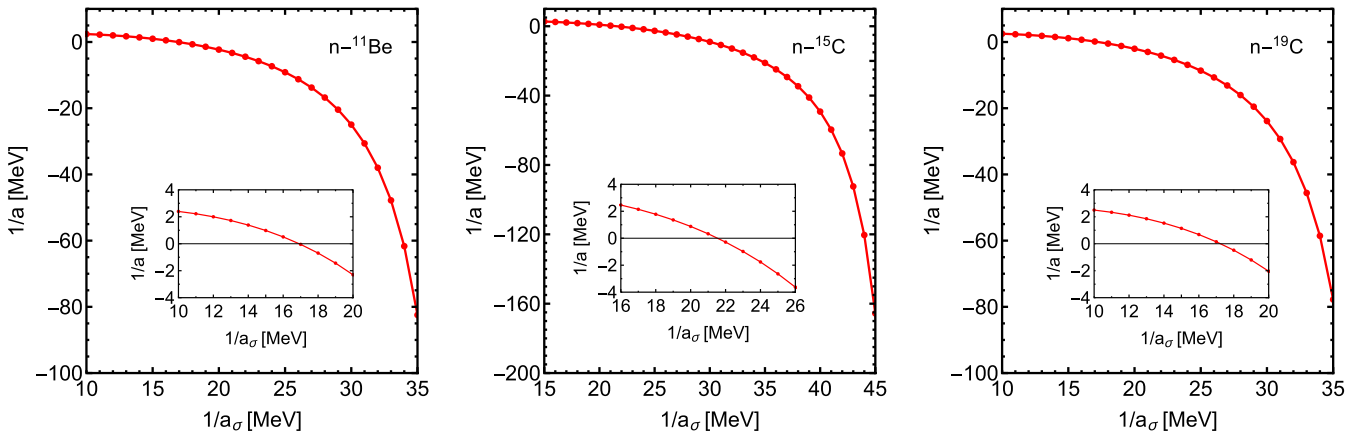

FIG. 12. Inverse of the scattering length $1/a$ of the s-wave scatterings of the neutron and one-neutron halo nuclei in the $J = 0$ channel: n-^{11}Be (left), n-^{15}C (middle), and n-^{19}C (right). The inset shows the transition of $1/a$ from positive to negative values in more detail.

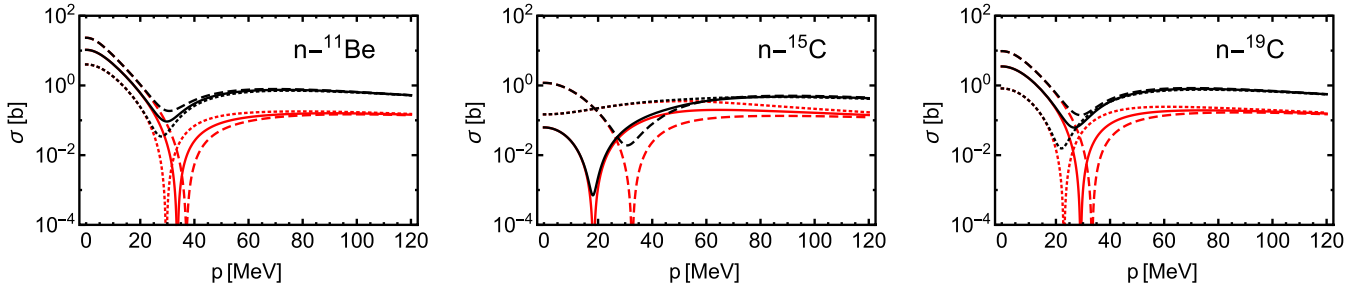

FIG. 13. Total cross sections considering only s-wave (red curves) and including higher partial waves with $l < 5$ (black curves) of the neutron and one-neutron halo nuclei in the $J = 0$ channel: n-^{11}Be (left), n-^{15}C (middle), and n-^{19}C (right). The notations of the solid, dashed, and dotted curves are the same as those in Fig. 6.

threshold are of the order of a few to ten barns for the n-^{11}Be and n-^{19}C scattering, and is much smaller (≈60 mb) for the n-^{15}C scattering. This is because is the latter case, the ^{16}C is more deeply bound than the other two cases and thus its enhancement effect at threshold is smaller.

We also find that for the neutron-core scattering length in a certain range, the s-wave neutron-halo-nucleus scattering amplitude has a zero, corresponding to a pole of $p\cot\delta_0^R$ near threshold on the real positive p axis. The location of the T-matrix zero depends on the neutron-core scattering length. This zero is a manifestation of the presence of an excited virtual Efimov state close to the scattering threshold. Our results for n-^{19}C scattering are in qualitative agreement with the work of Refs. [84] in the renormalized zero-range model. The qualitative features are unchanged by finite-range effects [85,86]. In contrast to Refs. [91,92], we find no evidence for a scattering resonance.

Up to higher order corrections, the position of the pole of $p\cot\delta_0^R$ is fully determined by the separation energies of the corresponding one- and two-neutron halo nuclei and the neutron-neutron scattering length. If it can be observed, e.g., through a minimum in the scattering cross section, it could serve as an experimental confirmation of Efimov physics in halo nuclei, even if bound excited states are absent. Thus it provides an alternative to previous proposals to observe the Efimov effect in halo nuclei [93] and the standard approach to observe excited states that satisfy the universal scaling relations [16,25,27,30,94]. While there is evidence that finite-range effects do not remove the minima [85,86], the calculation of higher-order corrections to their position would be valuable.

Despite the significant experimental challenges which the neutron-halo scattering approach poses, a theoretical exploration is nonetheless useful at this time. It is a basic ingredient of the scattering of one-neutron halo nuclei off deuteron targets, which is directly accessible in experiment. It would be interesting to elucidate whether the effects of virtual Efimov states in two-neutron halo nuclei persist in deuteron reactions by performing a four-body calculation.

ACKNOWLEDGMENTS

We are grateful to Han-Tao Jing and Shan-Gui Zhou for helpful discussions. This work is supported in part by the National Natural Science Foundation of China (NSFC) under Grants No. 12247139, 12125507, 11835015, and 12047503, by the Chinese Academy of Sciences (CAS) under Grants No. YSBR-101 and XDB34030000; by the NSFC and the Deutsche Forschungsgemeinschaft (DFG, German Research Foundation) through the funds provided to the Sino-German Collaborative Research Center "Symmetries and the Emergence of Structure in QCD" (NSFC Grant No. 12070131001, DFG Project-ID 196253076 - TRR110), by the DFG under Project-ID 279384907 - SFB 1245, and by the German Federal Ministry of Education and Research (BMBF) (Grant No. 05P21RDFNB).

APPENDIX A: LEGENDRE POLYNOMIALS OF THE SECOND KIND WITH COMPLEX ARGUMENT

The Legendre polynomials of the second kind with complex argument are

$$Q_0(z) = \frac{1}{2}\ln\frac{z+1}{z-1}, \tag{A1}$$

$$Q_1(z) = \frac{z}{2}\ln\frac{z+1}{z-1} - 1, \tag{A2}$$

$$Q_2(z) = \frac{1}{4}(3z^2-1)\ln\frac{z+1}{z-1} - \frac{3}{2}z, \tag{A3}$$

$$Q_3(z) = \frac{1}{4}(5z^3-3z)\ln\frac{z+1}{z-1} - \frac{5}{2}z^2 + \frac{2}{3}, \tag{A4}$$

$$Q_4(z) = \frac{1}{16}(35z^4-30z^2+3)\ln\frac{z+1}{z-1} - \frac{35}{8}z^3 + \frac{55}{24}z. \tag{A5}$$

APPENDIX B: NUMERICAL SOLUTION METHODO

The Faddeev equation can be solved using the matrix inversion method [95]. When the total energy E is above the two-body $n\sigma$ threshold, the σ dimer can be on-shell. And the logarithmic singularities in the s-wave projection core-exchange and neutron-exchange potentials in Eqs. (16) and (19) will also be in the integration region when E is above the three-body nnc threshold. Both of these will cause numerical instabilities as the integration in Eqs. (13) and (18) is performed along the positive real momentum axis. To overcome that problem, we use the contour deformation method [96–99]. The basic idea is that the integration contour in Eqs. (13) and (18) can be distorted from its original position

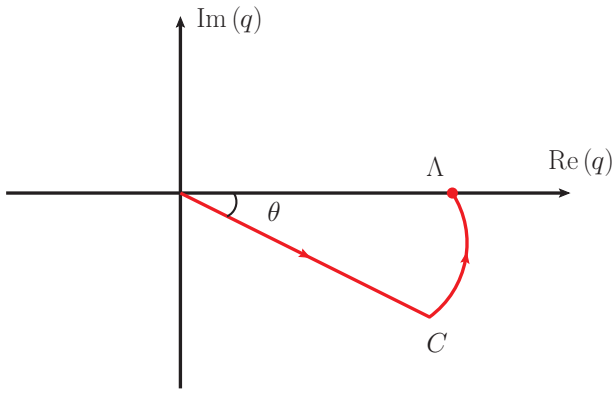

FIG. 14. The integration contour C for the evaluation of Eq. (B1).

along the positive real axis into the complex momentum plane without changing the results. One should note that the angle of the deformed contour should be large enough in order to avoid the singularities on the real axis but small enough in order not to cross the singularities in the core-exchange and neutron-exchange potentials. Using Cauchy's theorem, the relation between the solution of the Faddeev equation for real momentum and complex momentum can then be obtained.

To be concrete, we take the single channel case with $J = 1$ as an example, and the extension to the coupled-channel case is straightforward. First, the Faddeev equation is analytically continued into the complex momentum plane using Cauchy's theorem,

$$iT_{\sigma\sigma}(k', p, E) = iV_{\sigma\sigma}(k', p, E) - \int_C \frac{q'^2 dq'}{2\pi^2} V_{\sigma\sigma}(k', q', E) \times Z_\sigma^{-1} D_\sigma\left(E - \frac{q'^2}{2m_n}, q'\right) iT_{\sigma\sigma}(q', p, E), \tag{B1}$$

where k' and q' are complex momenta. And now the integration is along the deformed contour C, which will be discussed later. We can see that the Faddeev equation in Eq. (B1) is free of singularity for E on the real axis, and this equation can be solved using the matrix inversion method without any difficulty. The T matrix for real momentum k can then be obtained.

Since we are interested in the on-shell T matrix, we put the outgoing momentum k on the energy shell, which leads to

$$k = \left[2\mu_{n\sigma}\left(E + \frac{1}{2\mu_{nc}a_\sigma^2}\right)\right]^{1/2}, \tag{B2}$$

where $\mu_{n\sigma}$ is defined in Eq. (15). Inserting this into Eqs. (16) gives the logarithmic branch points of q satisfying

$$E - m_\sigma/(2m_n m_c)(q^2 + k^2) \pm qk/m_c + i\epsilon = 0, \tag{B3}$$

and the solutions of this equation give the locations of four branch points of q in the complex momentum plane,

$$q = \frac{\pm m_n k \pm i m_\sigma/a_\sigma}{m_\sigma}. \tag{B4}$$

In addition to these branch points, the dimer propagator has a pole at

$$q = \left[2\mu_{n\sigma}\left(E + \frac{1}{2\mu_{nc}a_\sigma^2} + i\epsilon\right)\right]^{1/2}. \tag{B5}$$

In our calculations, we rotate the integration contour into the lower half q plane, and q' is along the contour C as shown in Fig. 14 to avoid singularities in the dimer propagator and the core-exchange potential in Eq. (B1). The locations of the logarithmic branch points place an upper limit on θ, which is the angle between the clockwise-rotated integration path and the real q axis,

$$0 < \theta < \arctan\left(\frac{m_\sigma/a_\sigma}{m_n k}\right). \tag{B6}$$

We have checked that the numerical results are independent of the choice for θ as long as its value satisfies the above constraint.

[1] M. V. Zhukov, B. V. Danilin, D. V. Fedorov, J. M. Bang, I. J. Thompson, and J. S. Vaagen, Bound state properties of Borromean halo nuclei: He-6 and Li-11, Phys. Rep. **231**, 151 (1993).

[2] A. S. Jensen, K. Riisager, D. V. Fedorov, and E. Garrido, Structure and reactions of quantum halos, Rev. Mod. Phys. **76**, 215 (2004).

[3] B. Jonson, Light dripline nuclei, Phys. Rep. **389**, 1 (2004).

[4] I. Tanihata, H. Savajols, and R. Kanungo, Recent experimental progress in nuclear halo structure studies, Prog. Part. Nucl. Phys. **68**, 215 (2013).

[5] S. Weinberg, Nuclear forces from chiral lagrangians, Phys. Lett. B **251**, 288 (1990).

[6] S. Weinberg, Effective chiral lagrangians for nucleon-pion interactions and nuclear forces, Nucl. Phys. B **363**, 3 (1991).

[7] S. R. Beane, P. F. Bedaque, W. C. Haxton, D. R. Phillips, and M. J. Savage, From hadrons to nuclei: Crossing the border, arXiv:nucl-th/0008064.

[8] P. F. Bedaque and U. van Kolck, Effective field theory for few nucleon systems, Annu. Rev. Nucl. Part. Sci. **52**, 339 (2002).

[9] E. Epelbaum, Few-nucleon forces and systems in chiral effective field theory, Prog. Part. Nucl. Phys. **57**, 654 (2006).

[10] E. Epelbaum, H.-W. Hammer, and Ulf-G. Meißner, Modern theory of nuclear forces, Rev. Mod. Phys. **81**, 1773 (2009).

[11] S. K. Bogner, R. J. Furnstahl, and A. Schwenk, From low-momentum interactions to nuclear structure, Prog. Part. Nucl. Phys. **65**, 94 (2010).

[12] R. Machleidt and D. R. Entem, Chiral effective field theory and nuclear forces, Phys. Rep. **503**, 1 (2011).

[13] H.-W. Hammer, A. Nogga, and A. Schwenk, Three-body forces: From cold atoms to nuclei, Rev. Mod. Phys. **85**, 197 (2013).

[14] J. W. Holt, M. Rho, and W. Weise, Chiral symmetry and effective field theories for hadronic, nuclear and stellar matter, Phys. Rep. **621**, 2 (2016).

[15] T. Papenbrock and H. A. Weidenmüller, Effective field theory for deformed atomic nuclei, Phys. Scr. **91**, 053004 (2016).

[16] H.-W. Hammer, C. Ji, and D. R. Phillips, Effective field theory description of halo nuclei, J. Phys. G: Nucl. Part. Phys. **44**, 103002 (2017).

[17] H.-W. Hammer, S. König, and U. van Kolck, Nuclear effective field theory: Status and perspectives, Rev. Mod. Phys. **92**, 025004 (2020).

[18] C. A. Bertulani, H. W. Hammer, and U. Van Kolck, Effective field theory for halo nuclei, Nucl. Phys. A **712**, 37 (2002).

[19] P. F. Bedaque, H. W. Hammer, and U. van Kolck, Narrow resonances in effective field theory, Phys. Lett. B **569**, 159 (2003).

[20] R. Higa, H.-W. Hammer, and U. van Kolck, Alpha alpha scattering in halo effective field Theory, Nucl. Phys. A **809**, 171 (2008).

[21] V. Efimov, Energy levels arising form the resonant two-body forces in a three-body system, Phys. Lett. B **33**, 563 (1970).

[22] V. Efimov, Weakly-bound states of three resonantly-interacting particles, Sov. J. Nucl. Phys. **12**, 589 (1971) [Yad. Fiz. **12**, 1080 (1970)].

[23] R. D. Amado and J. V. Noble, On Efimov's effect: A new pathology of three-particle systems, Phys. Lett. B **35**, 25 (1971).

[24] R. D. Amado and J. V. Noble, Efimov's effect - A new pathology of three-particle systems. II, Phys. Rev. D **5**, 1992 (1972).

[25] D. V. Fedorov, A. S. Jensen, and K. Riisager, Efimov states in halo nuclei, Phys. Rev. Lett. **73**, 2817 (1994).

[26] A. J. E. Nielsen, D.V. Fedorov and E. Garrido, The three-body problem with short-range interactions, Phys. Rep. **347**, 373 (2001).

[27] A. E. A. Amorim, T. Frederico, and L. Tomio, Universal aspects of Efimov states and light halo nuclei, Phys. Rev. C **56**, R2378 (1997).

[28] E. Braaten and H.-W. Hammer, Universality in few-body systems with large scattering length, Phys. Rep. **428**, 259 (2006).

[29] P. Naidon and S. Endo, Efimov Physics: A review, Rep. Prog. Phys. **80**, 056001 (2017).

[30] D. L. Canham and H.-W. Hammer, Universal properties and structure of halo nuclei, Eur. Phys. J. A **37**, 367 (2008).

[31] P. Hagen, H.-W. Hammer, and L. Platter, Charge form factors of two-neutron halo nuclei in halo EFT, Eur. Phys. J. A **49**, 118 (2013).

[32] B. Acharya, C. Ji, and D. R. Phillips, Implications of a matter-radius measurement for the structure of carbon-22, Phys. Lett. B **723**, 196 (2013).

[33] C. Ji, C. Elster, and D. R. Phillips, ^{6}He nucleus in halo effective field theory, Phys. Rev. C **90**, 044004 (2014).

[34] J.-Y. Pang, L.-T. Li, F.-K. Guo, and J.-J. Wu, Three-body coupled channel framework for two-neutron halo nuclei, arXiv:2301.07296 [nucl-th] (2023).

[35] D. L. Canham and H.-W. Hammer, Range corrections for two-neutron halo nuclei in effective theory, Nucl. Phys. A **836**, 275 (2010).

[36] J. Vanasse, Charge and matter form factors of two-neutron halo nuclei in halo effective field theory at next-to-leading-order, Phys. Rev. C **95**, 024318 (2017).

[37] H.-W. Hammer and D. R. Phillips, Electric properties of the beryllium-11 system in halo EFT, Nucl. Phys. A **865**, 17 (2011).

[38] G. Rupak and R. Higa, Model-independent calculation of radiative neutron capture on lithium-7, Phys. Rev. Lett. **106**, 222501 (2011).

[39] G. Rupak, L. Fernando, and A. Vaghani, Radiative neutron capture on carbon-14 in effective field theory, Phys. Rev. C **86**, 044608 (2012).

[40] B. Acharya and D. R. Phillips, Carbon-19 in halo EFT: Effective-range parameters from coulomb-dissociation experiments, Nucl. Phys. A **913**, 103 (2013).

[41] X. Zhang, K. M. Nollett, and D. R. Phillips, Marrying ab initio calculations and halo-EFT: the case of $^7\mathrm{Li} + n \to {}^8\mathrm{Li} + \gamma$, Phys. Rev. C **89**, 024613 (2014).

[42] X. Zhang, K. M. Nollett, and D. R. Phillips, Halo effective field theory constrains the solar $^7Be + p \to {}^8B + \gamma$ rate, Phys. Lett. B **751**, 535 (2015).

[43] X. Zhang, K. M. Nollett, and D. R. Phillips, *S*-factor and scattering-parameter extractions from $^3\mathrm{He} + {}^4\mathrm{He} \to {}^7\mathrm{Be} + \gamma$, J. Phys. G: Nucl. Part. Phys. **47**, 054002 (2020).

[44] M. Göbel, B. Acharya, H.-W. Hammer, and D. R. Phillips, Final-state interactions and spin structure in E1 breakup of Li11 in halo effective field theory, Phys. Rev. C **107**, 014617 (2023).

[45] H.-W. Hammer, Theory of halo nuclei (2022) arXiv:2203.13074 [nucl-th].

[46] TUNL nuclear data evaluation project.

[47] F. Ajzenberg-Selove, Energy levels of light nuclei A = 18–20, Nucl. Phys. A **475**, 1 (1987).

[48] F. Ajzenberg-Selove, Energy levels of light nuclei A = 13–15, Nucl. Phys. A **523**, 1 (1991).

[49] D. R. Tilley, J. H. Kelley, J. L. Godwin, D. J. Millener, J. E. Purcell, C. G. Sheu, and H. R. Weller, Energy levels of light nuclei A = 8,9,10, Nucl. Phys. A **745**, 155 (2004).

[50] W. J. Huang, M. Wang, F. G. Kondev, G. Audi, and S. Naimi, The AME 2020 atomic mass evaluation (I). Evaluation of input data, and adjustment procedures, Chin. Phys. C **45**, 030002 (2021).

[51] M. Wang, W. J. Huang, F. G. Kondev, G. Audi, and S. Naimi, The AME 2020 atomic mass evaluation (II). Tables, graphs and references, Chin. Phys. C **45**, 030003 (2021).

[52] L. Fernando, A. Vaghani, and G. Rupak, Electromagnetic form factors of one neutron halos with spin 1/2+ ground state, arXiv:1511.04054 [nucl-th] (2015).

[53] L. Moschini, J. Yang, and P. Capel, ^{15}C: From halo effective field theory structure to the study of transfer, breakup, and radiative-capture reactions, Phys. Rev. C **100**, 044615 (2019).

[54] W. L. Zhan, H. S. Xu, G. Q. Xiao, J. W. Xia, H. W. Zhao, and Y. J. Yuan (HIRFL-CSR Group), Progress in HIRFL-CSR, Nucl. Phys. A **834**, 694c (2010).

[55] S. Gales, SPIRAL2 at GANIL: Next generation of ISOL facility for intense secondary radioactive ion beams, Nucl. Phys. A **834**, 717c (2010).

[56] T. Motobayashi, RIKEN RI Beam Factory – Recent results and perspectives, Nucl. Phys. A **834**, 707c (2010).

[57] M. Thoennessen, Plans for the facility for rare isotope beams, Nucl. Phys. A **834**, 688c (2010).

[58] X. Zhou and J. Yang (HIAF Project Team), Status of the high-intensity heavy-ion accelerator facility in China, AAPPS Bull. **32**, 35 (2022).

[59] J. Wei *et al.*, China Spallation Neutron Source Design, R&D, and outlook, Nucl. Instrum. Methods A **600**, 10 (2009).

[60] H. Chen and X.-L. Wang, China's first pulsed neutron source, Nat. Mater. **15**, 689 (2016).

[61] R. L. Workman *et al.* (Particle Data Group), Review of particle physics, PTEP **2022**, 083C01 (2022).

[62] P. F. Bedaque and U. van Kolck, Nucleon deuteron scattering from an effective field theory, Phys. Lett. B **428**, 221 (1998).

[63] P. F. Bedaque, H. W. Hammer, and U. van Kolck, Effective theory for neutron deuteron scattering: Energy dependence, Phys. Rev. C **58**, R641 (1998).

[64] P. F. Bedaque, H. W. Hammer, and U. van Kolck, Effective theory of the triton, Nucl. Phys. A **676**, 357 (2000).

[65] D. B. Kaplan, M. J. Savage, and M. B. Wise, A New expansion for nucleon-nucleon interactions, Phys. Lett. B **424**, 390 (1998).

[66] D. B. Kaplan, M. J. Savage, and M. B. Wise, Two nucleon systems from effective field theory, Nucl. Phys. B **534**, 329 (1998).

[67] Q. Chen *et al.*, Measurement of the neutron-neutron scattering length using the $\pi^- d$ capture reaction, Phys. Rev. C **77**, 054002 (2008).

[68] H. A. Bethe, Theory of the effective range in nuclear scattering, Phys. Rev. **76**, 38 (1949).

[69] P. F. Bedaque and H. W. Griesshammer, Quartet S wave neutron deuteron scattering in effective field theory, Nucl. Phys. A **671**, 357 (2000).

[70] P. F. Bedaque, G. Rupak, H. W. Griesshammer, and H.-W. Hammer, Low-energy expansion in the three-body system to all orders and the triton channel, Nucl. Phys. A **714**, 589 (2003).

[71] H. W. Griesshammer, Improved convergence in the three-nucleon system at very low energies, Nucl. Phys. A **744**, 192 (2004).

[72] G. Skorniakov and K. Ter-Martirosian, Three body problem for short range forces 1. Scattering of low energy neutrons by deuterons, Sov. Phys. JETP **4**, 648 (1957) [J. Exptl. Theoret. Phys. (USSR) **31**, 775 (1956)].

[73] L. Faddeev, Scattering theory for a three particle system, Sov. Phys. JETP **12**, 1014 (1961) [J. Exptl. Theoret. Phys. (USSR) **39**, 1459 (1960)].

[74] G. Danilov, On the three-body problem with short-range forces, Sov. Phys. JETP **13**, 349 (1961) [J. Exptl. Theoret. Phys. (USSR) **40**, 498 (1961)].

[75] L. F. R.A. Minlos, On the three-body problem with short-range forces, Sov. Phys. JETP **14**, 1315 (1962) [J. Exptl. Theoret. Phys. (USSR) **41**, 1580 (1961)].

[76] G. Danilov, On the three-body problem with short-range forces, Sov. Phys. JETP **17**, 1015 (1963) [J. Exptl. Theoret. Phys. (USSR) **44**, 1509 (1963)].

[77] P. F. Bedaque, H. W. Hammer, and U. van Kolck, Renormalization of the three-body system with short range interactions, Phys. Rev. Lett. **82**, 463 (1999).

[78] R. F. Mohr, R. J. Furnstahl, R. J. Perry, K. G. Wilson, and H.-W. Hammer, Precise numerical results for limit cycles in the quantum three-body problem, Ann. Phys. **321**, 225 (2006).

[79] N. Isgur and M. B. Wise, Weak decays of heavy mesons in the static quark approximation, Phys. Lett. B **232**, 113 (1989).

[80] E. E. Jenkins and A. V. Manohar, Baryon chiral perturbation theory using a heavy fermion Lagrangian, Phys. Lett. B **255**, 558 (1991).

[81] V. Bernard, N. Kaiser, and U.-G. Meißner, Chiral dynamics in nucleons and nuclei, Int. J. Mod. Phys. E **04**, 193 (1995).

[82] P. F. Bedaque, H. W. Hammer, and U. van Kolck, The three boson system with short range interactions, Nucl. Phys. A **646**, 444 (1999).

[83] M. L. Goldberger and K. M. Watson, *Collision Theory* (John Wiley & Sons, New York, 1964).

[84] M. T. Yamashita, T. Frederico, and L. Tomio, Neutron–^{19}C scattering near an Efimov state, Phys. Lett. B **670**, 49 (2008).

[85] M. A. Shalchi, M. T. Yamashita, M. R. Hadizadeh, T. Frederico, and L. Tomio, Neutron− ^{19}C scattering: Emergence of universal properties in a finite range potential, Phys. Lett. B **764**, 196 (2017); **771**, 635 (2017).

[86] A. Deltuva, Neutron– 19 C scattering: Towards including realistic interactions, Phys. Lett. B **772**, 657 (2017).

[87] M.-L. Du, A. Filin, V. Baru, X.-K. Dong, E. Epelbaum, F.-K. Guo, C. Hanhart, A. Nefediev, J. Nieves, and Q. Wang, Role of left-hand cut contributions on pole extractions from lattice data: Case study for $T_{cc}(3875)^+$, Phys. Rev. Lett. **131**, 131903 (2023).

[88] A. C. Phillips and G. Barton, Relations between low-energy three nucleon observables, Phys. Lett. B **28**, 378 (1969).

[89] A. S. Reiner, On the anomalous effective range expansion for nucleon-deuteron scattering in the $S = 1/2$ state, Phys. Lett. B **28**, 387 (1969).

[90] G. Rupak, A. Vaghani, R. Higa, and U. van Kolck, Fate of the neutron–deuteron virtual state as an Efimov level, Phys. Lett. B **791**, 414 (2019).

[91] I. Mazumdar, A. R. P. Rau, and V. S. Bhasin, Efimov states and their Fano resonances in a neutron-rich nucleus, Phys. Rev. Lett. **97**, 062503 (2006).

[92] I. Mazumdar, V. S. Bhasin, and A. R. P. Rau, Evolution of Efimov states into the continuum in neutron rich (2n-core) nuclei: A general study, Phys. Lett. B **704**, 51 (2011).

[93] A. O. Macchiavelli, How to study Efimov states in exotic nuclei?, Few-Body Syst. **56**, 773 (2015).

[94] J. Bishop *et al.*, Evidence against the Efimov effect in ^{12}C from spectroscopy and astrophysics, Phys. Rev. C **103**, L051303 (2021).

[95] M. I. Haftel and F. Tabakin, Nuclear saturation and the smoothness of nucleon-nucleon potentials, Nucl. Phys. A **158**, 1 (1970).

[96] J. Hetherington and L. Schick, Exact multiple-scattering analysis of low-energy elastic $K^- - d$ scattering with separable potentials, Phys. Rev. **137**, B935 (1965).

[97] R. Aaron and R. D. Amado, Theory of the reaction $n + d \to n + n + p$, Phys. Rev. **150**, 857 (1966).

[98] R. T. Cahill and I. H. Sloan, Theory of neutron-deuteron breakup at 14.4 MeV, Nucl. Phys. A **165**, 161 (1971), **196**, 632 (1972).

[99] E. Schmid and H. Ziegelmann, *The Quantum Mechanical Three-Body Problem* (Pergamon Press, Oxford, 1974).